Structure and Dynamics of Halogenoethanol−Water Mixtures Studied by Large-Angle X-ray Scattering, Small-Angle Neutron Scattering, and NMR Relaxation

ARTICLE *in* THE JOURNAL OF PHYSICAL CHEMISTRY A · SEPTEMBER 2005

Impact Factor: 2.69 · DOI: 10.1021/jp051470o · Source: PubMed

5 AUTHORS, INCLUDING:

Toshiyuki Takamuku
Saga University
84 PUBLICATIONS **1,922** CITATIONS
SEE PROFILE

Koji Yoshida
Fukuoka University
62 PUBLICATIONS **682** CITATIONS
SEE PROFILE

Toshiya Otomo
High Energy Accelerator Research Organization
139 PUBLICATIONS **1,165** CITATIONS
SEE PROFILE

Toshio Yamaguchi
Fukuoka University
203 PUBLICATIONS **3,783** CITATIONS
SEE PROFILE

Structure and Dynamics of Halogenoethanol−Water Mixtures Studied by Large-Angle X-ray Scattering, Small-Angle Neutron Scattering, and NMR Relaxation

Toshiyuki Takamuku,*,† Takashi Kumai,† Koji Yoshida,‡ Toshiya Otomo,§ and Toshio Yamaguchi‡

Department of Chemistry and Applied Chemistry, Faculty of Science and Engineering, Saga University, Honjo-machi, Saga 840-8502, Japan, Advanced Material Institute and Department of Chemistry, Faculty of Science, Fukuoka University, Nanakuma, Jonan-ku, Fukuoka 814-0180, Japan, and Institute of Materials Structure Science, High Energy Accelerator Research Organization (KEK), Oho, Tsukuba 305-0801, Japan

Received: March 21, 2005; In Final Form: May 25, 2005

To clarify the structure of solvent clusters formed in halogenoethanol−water mixtures at the molecular level, large-angle X-ray scattering (LAXS) measurements have been made at 298 K on 2,2,2-trifluoroethanol (TFE), 2,2,2-trichloroethanol (TCE), and their aqueous mixtures in the TFE and TCE mole fraction ranges of $0.002 \leq x_{TFE} \leq 0.9$ and $0.5 \leq x_{TCE} \leq 0.9$, respectively. The radial distribution functions (RDFs) for TFE−water mixtures have shown that the structural transition from inherent TFE structure to the tetrahedral-like structure of water takes place at $x_{TFE} \approx 0.2$. In the TCE−water mixtures inherent TCE structure remains in the range of $0.5 \leq x_{TCE} \leq 1$. Small-angle neutron scattering (SANS) experiments have been performed on CF_3CH_2-OD− (TFE-d_1−) D_2O and CF_3CD_2OH− (TFE-d_2−) H_2O mixtures in the TFE mole fraction range of $0.05 \leq x_{TFE} \leq 0.8$. The SANS results in terms of the Ornstein−Zernike correlation length have revealed that TFE and water molecules are most heterogeneously mixed with each other in the TFE−water mixture at $x_{TFE} \approx 0.15$, i.e., both TFE clusters and water clusters are most enhanced in the mixture. To evaluate the dynamics of TFE and ethanol (EtOH) molecules in TFE−water and ethanol−water mixtures, respectively, ^{1}H NMR relaxation rates for the methylene group within alcohol molecules have been measured by using an inversion-recovery method. The alcohol concentration dependence of the relaxation rates for the TFE−water and ethanol−water mixtures has shown a break point at $x_{TFE} \approx 0.15$ and $x_{EtOH} \approx 0.2$, respectively, where the structural transition from alcohol clusters to the tetrahedral-like structure of water takes place. On the basis of the present results, the most likely structure models of solvent clusters predominantly formed in TFE−water and TCE−water mixtures are proposed. In addition, effects of halogenation of the hydrophobic groups on clustering of alcohol molecules are discussed from the present results, together with the previous ones for ethanol−water and 1,1,1,3,3,3-hexafluoro-2-propanol− (HFIP−) water mixtures.

Introduction

Halogeno alcohols, such as TFE[1−7] and HFIP,[8] have often been used in the fields of biochemistry and biophysics to investigate functions of peptides and proteins because they promote α-helical structure of peptides and proteins in aqueous solution more strongly than aliphatic alcohols, such as ethanol and 2-propanol. However, the underlying mechanism of alcohol-induced α-helix formation and denaturation of peptides and proteins has not yet been well understood at the molecular level. So far, the mechanism has frequently been discussed in terms of changes in dielectric constant and pH of aqueous peptide and protein solutions by addition of alcohol. Recently, it has been reported that solvent clusters formed in alcohol−water mixtures are an important factor for the alcohol-induced α-helical structure of peptides and proteins.[9−11]

In a previous investigation, we have clarified the structure and dynamics of HFIP−water binary mixtures by using LAXS, SANS, NMR, and mass spectrometry.[12] On the basis of all the results, it has been concluded that the tetrahedral-like structure of water is mainly formed in the HFIP−water mixtures in the range of HFIP mole fraction $x_{HFIP} \leq \sim 0.1$, while inherent HFIP structure is gradually evolved in the mixtures with increasing HFIP mole fraction in the rage of $x_{HFIP} \geq \sim 0.15$, i.e., the structural transition from inherent HFIP structure to the tetrahedral-like structure of water takes place at $x_{HFIP} \approx 0.1$. In particular, the SANS experiment on HFIP−D_2O mixtures at various x_{HFIP} has suggested that clustering and microheterogeneity in the mixtures are most enhanced at $x_{HFIP} \approx 0.06$. This is in good agreement with the investigation by Goto and co-workers.[11] Their results of small-angle X-ray scattering (SAXS) measurements have shown that clustering of TFE and HFIP molecules is most progressed in TFE−water and HFIP−water mixtures at 30% (v/v) of alcohol, which corresponds to a HFIP mole fraction of $x_{HFIP} \approx 0.06$, and the clustering is strongly related to the promotion of the α-helical structure of β-lactoglobulin and melittin. For other halogeno alcohols, it has been reported that TCE, monochloroethanol, and dichloroethanol molecules strongly interact with proteins in aqueous mixtures.[13,14] Moreover, the effect of alcohol-induced secondary structure of peptides and proteins increases in the order of monobromoethanol > monochloroethaol > monofluoroethanol.[10,14] However, detailed structures of halogeno alcohol−water mixtures

* To whom all correspondence should be addressed. E-mail: takamut@cc.saga-u.ac.jp.
† Saga University.
‡ Fukuoka University.
§ High Energy Accelerator Research Organization (KEK).

10.1021/jp051470o CCC: $30.25
Published on Web 08/09/2005

have not yet been clarified at the molecular level, except for that of HFIP−water mixtures in the previous investigation.[12]

In the present investigation, to clarify the structure and dynamics of pure TFE and TFE−water over the TFE mole fraction range of $0.002 \leq x_{TFE} \leq 0.9$, LAXS, SANS, and ^{1}H NMR relaxation experiments at 298 K have been made on TFE and TFE−water mixtures. LAXS measurements at 298 K have been performed on TCE and TCE−water mixtures in a limited TCE mole fraction range of $0.5 \leq x_{TCE} < 1$ because TCE is immiscible at 298 K with water when $x_{TCE} < 0.5$. From these results the most likely structural changes in dominant solvent clusters formed in TFE−water and TCE−water mixtures with alcohol mole fraction are proposed. In addition, effects of the halogenation of the hydrophobic group on clustering of alcohol molecules are discussed from the present results, together with the previous ones for ethanol−water[15−17] and HFIP−water mixtures.[12]

Experimental Section

Sample Solutions. TFE (Tokyo Kasei Industry, extra grade), TCE (Tokyo Kasei Industry, extra grade), and ethanol (Wako Pure Chemicals, grade for high performance liquid chromatography) were dried with thermally activated 4 Å molecular sieves for several days. Doubly distilled water was used for LAXS and NMR relaxation experiments. For the SANS experiments, TFE-d_1 (Aldrich, D atom content of 99.5%), TFE-d_2 (ISOTEC, D atom content of 99.5%), and D_2O (Aldrich, D atom content of 99.9%) were used without further purification. Sample solutions of the alcohol−water mixtures were prepared by weighing alcohol and water to the required alcohol mole fractions.

LAXS Measurements. LAXS measurements at 298 K were made on pure TFE and TFE−water mixtures at $x_{TFE} = 0.002$, 0.01, 0.05, 0.1, 0.2, 0.3, 0.4, 0.5, 0.6, 0.7, 0.8, and 0.9 and pure TCE and TCE−water mixtures at $x_{TCE} = 0.5$, 0.6, 0.7, 0.8, and 0.9. The TCE−water mixtures at $x_{TCE} < 0.5$ were not available since both solvents are not miscible in this range. A rapid liquid X-ray diffractometer (BRUKER AXS, model DIP301) with an imaging plate (IP) (Fuji Film Co.) as a two-dimensional detector were used in the present LAXS experiments. Details of X-ray diffractometer have been described elsewhere.[18,19] Densities for the sample solutions were measured at 298 K by using a densimeter (Anton Paar K.G., DMA60). X-rays were generated at a rotary Mo anode (Rigaku, RU-300) operated at 50 kV and 200 mA, and then monochromatized by a flat graphite crystal to obtain MoKα radiation (the wavelength $\lambda = 0.7107$ Å). X-ray scattering intensities for a sample solution sealed in a glass capillary of 2 mm inner diameter (wall thickness 0.01 mm) were accumulated on the IP for 1 h. The observed range of the scattering angle (2θ) was 0.2° to 109°, corresponding to the scattering vector s ($=4\pi\lambda^{-1} \sin\theta$) of 0.03−14.4 Å^{-1}. X-ray intensities for an empty capillary were also measured as background.

Two-dimensional X-ray data, $I_{obsd}(x, y)$, where x and y are horizontal and vertical coordinates, measured on the IP were integrated into one-dimensional data, $I_{obsd}(\theta)$, after correction for polarization as previously reported.[18] The observed intensities for the samples and empty capillary were also corrected for absorption.[19] The contribution of the sample solution alone was obtained by subtracting the intensities for the empty capillary from those for the sample. The corrected intensities were normalized to absolute units by conventional methods.[20−22] The structure function, $i(s)$, was calculated by using eq 1 in ref 23. In the data treatment the stoichiometric volume V was chosen to contain one O atom from both TFE or TCE and water in the systems. The structure function was Fourier transformed into the radial distribution function, $D(r)$, in a usual manner.[23] To perform a quantitative analysis of the X-ray data, a comparison between the experimental structure function and the theoretical one, which was calculated on a structure model with eq 5 in ref 23, was made by a least-squares refinement procedure by using eq 4 in ref 23. The present X-ray diffraction data were treated by programs KURVLR[24] and NLPLSQ.[25]

SANS Measurements. TFE-d_1−D_2O mixtures at $x_{TFE} = 0.05$, 0.08, 0.1, 0.13, 0.18, 0.2, 0.4, and 0.6 were prepared in a nitrogen-filled glovebox to avoid replacing D atoms with H ones. Preparation of TFE-d_2−H_2O mixtures at $x_{TFE} = 0.05$, 0.08, 0.1, 0.13, 0.18, 0.2, 0.4, 0.6, and 0.8 was made under an ambient condition. SANS measurements on the sample solutions were made on the SWAN spectrometer at a pulsed neutron facility (KENS) of the High Energy Accelerator Research Organization (KEK), Tsukuba, Japan. The momentum transfer Q ($= 4\pi\lambda^{-1}\sin\theta$) range covered with SWAN was 0.01−12 Å^{-1}.[26] The sample solutions were kept in a quartz cell of 22 mm in width, 25 mm in height, and 2 mm in sample thickness. The temperature was kept at 298.2 ± 0.5 K. The neutron beam size at a sample position was 20 × 20 mm^2, and the wavelength range used was $\lambda = 1-16$ Å. The scattering intensities were accumulated for 3−4 h per sample. The observed intensities were corrected for background, absorption, and cell scattering. The transmission by a sample and a cell was measured with ^{3}He position sensitive detector placed at a beam stopper position. The correction for detector efficiencies and normalization to absolute units was made by dividing the intensities of each solution by those of vanadium.[26] The incoherent scattering was subtracted from the normalized intensities. All parameter values required for the above corrections were taken from the literature.[27]

^{1}H NMR Relaxation Measurements. ^{1}H spin−lattice relaxation time, T_1, of alcohol molecules in the TFE−water and ethanol−water mixtures was measured on an FT-NMR spectrometer (JEOL, JNM-AL300). The sample solution was kept in 5 mm sample tube (Shigemi, PS-001) and degassed by five freeze−pump−thaw cycles before measurements. The probe temperature was controlled at 298.2 ± 0.1 K by a mixture of hot air and a dry nitrogen stream from liquid nitrogen. T_1 was measured by an inversion−recovery method with a pulse sequence $(\pi-\tau-\pi/2)^n$, where the number n of the delay times τ in the series of the sequence was 13 for the present experiments. The longest delay time exceeded $5T_1$. The T_1 data for each sample solution were measured three times and averaged to give a final value. The observed frequency range was 600 or 1000 Hz; sampling points were 2048 or 4096; the digital resolution range was 0.488−0.586 Hz.

Results and Discussion

LAXS for TFE—Water Mixtures. Figure 1 shows the s-weighted structure functions $i(s)$ for pure TFE and the TFE−water mixtures in the TFE mole fraction range of $0.002 \leq x_{TFE} \leq 0.9$, together with that of pure water[28] for comparison. Figure 2 indicates the corresponding RDFs in the $D(r)$-$4\pi r^2\rho_0$ form.

In the RDF for pure TFE ($x_{TFE} = 1$), two dominant peaks at 1.4 and 2.3 Å are assigned to intramolecular $C_2-F(F_1, F_2, F_3)$, C_1-O, and C_1-C_2 bonds and $C_1\cdots F$ and $F\cdots F$ nonbonding interactions within a TFE molecule, respectively (the notation of the atoms is shown in Figure 3). A small peak at 2.8 Å arises from the nearest-neighbor O···O hydrogen bonds between TFE molecules. According to an LAXS investigation on pure TFE by Radnai et al.[29] a TFE molecule may possess two conforma-

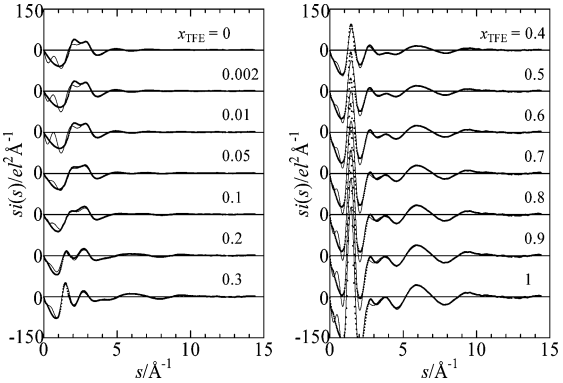

Figure 1. Structure functions $i(s)$ multiplied by s for TFE, water, and TFE−water mixtures at various x_{TFE}. Dotted lines represent experimental values, and solid lines are theoretical ones.

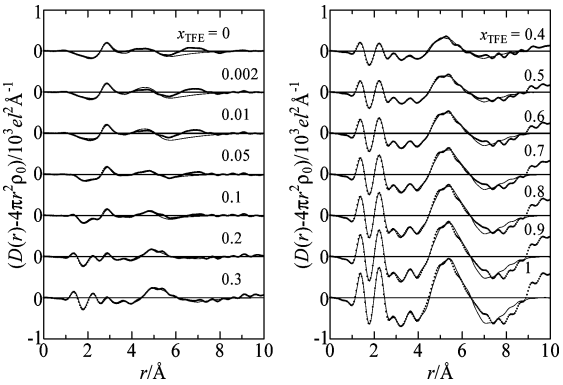

Figure 2. RDFs in the $D(r)$-$4\pi r^2\rho_0$ form for TFE, water, and TFE−water mixtures at various x_{TFE}. Dotted lines represent experimental values, and solid lines are theoretical ones.

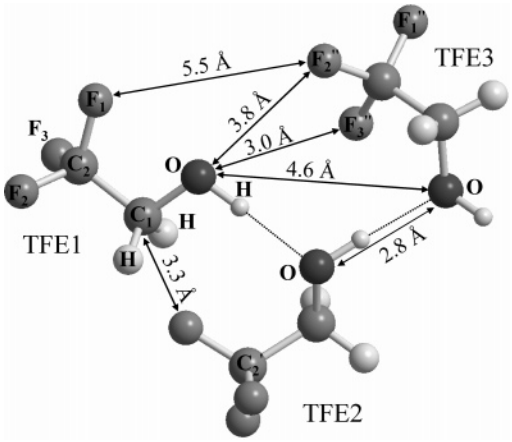

Figure 3. Structural model of TFE trimer.

tions, *g*-staggered and *g*-eclipsed ones, where the F_3 atom is positioned in trans and cis positions against the hydroxyl group, respectively, a small peak at 3.6 Å can be assigned to O···F_3 and O···$F_{2,3}$ intramolecular interactions for *g*-staggered and *g*-eclipsed conformers of TFE molecule.[29] A large and broad peak centered at 5.5 Å is attributed to the first- and second-neighbor interactions among TFE molecules as described below. Furthermore, the interactions in the range of $8 \le r/Å \le 10$ arise from the third- and fourth-neighbor interactions between TFE molecules. These features of the RDF for TFE are comparable with those for ethanol, although the third- and fourth-neighbor interactions between TFE molecules appear in the longer-range than those ($7 \le r/Å \le 10$) between ethanol molecules[15−17] because of the more significant contribution of F atoms in the CF_3 group than H ones in the CH_3 group. It is thus suggested that TFE molecules form hydrogen-bonded clusters as well as ethanol ones.

TABLE 1: Intramolecular Interactions for TFE and Water Molecules[a]

interaction	r	10^3b	n
	2,2,2-Trifluoroethanol		
O−H	0.960	2	1
C_1−H	1.085	1	2
C_2−F	1.360	2	3
C_1−O	1.402	3	1
C_1−C_2	1.526	2	1
H···H	1.770	5	1
C_2···H	2.130	5	2
F···F	2.144	3	3
C_1···F	2.380	5	3
C_2···O	2.390	8	1
	g-Staggered Conformer		
O···F_1,F_2	2.780	10	1
O···F_3	3.460	25	0.5
	g-Eclipsed Conformer		
O···F_1	2.400	20	0.5
O···F_2,F_3	3.230	15	1
	Water[b]		
O−H	0.970	2	2
H···H	1.555	10	1

[a] The distance r(Å), temperature factor b(Å^2), and number n. [b] Ref 32.

In the RDF for pure water ($x_{TFE} = 0$), three peaks at 2.8, 4.5, and 7 Å are observed, corresponding to the first-, second-, and third-neighbor molecules in the hydrogen-bonded network of water as reported in the literature.[30,31]

For the TFE−water mixtures, the RDFs in the range of $0.4 \le x_{TFE} \le 0.9$ are comparable with that for pure TFE, though the intensities of the peaks gradually decrease with decreasing TFE mole fraction. This shows that inherent TFE structure is dominant in the mixtures in the range of $0.4 \le x_{TFE} \le 0.9$. In this mole fraction range, the 2.8 Å peak for O···O hydrogen bonds scarcely changes when the x_{TFE} decreases. At $x_{TFE} = 0.2$ and 0.3 the third- and forth-neighbor interactions of TFE molecules at $8 \le r/Å \le 10$ almost disappear, but the first- and second-neighbor ones centered at ∼5 Å are still observed, showing that inherent TFE structure is considerably distorted in the mixtures. When the x_{TFE} further decreases to 0.1, the 2.8 Å peak for O···O hydrogen bonds is significantly grown. In addition, the peak at ∼5 Å observed in the RDFs at $x_{TFE} \ge 0.2$ shifts to the shorter distance ∼4.5 Å. At $x_{TFE} \le 0.1$ a new peak appears at 7 Å, and the RDFs are comparable with that for pure water. These features suggest that the tetrahedral-like structure of water is enhanced in the TFE−water mixtures when $x_{TFE} \le 0.1$, whereas inherent TFE structure almost disappears in the mixtures. Consequently, the present results of the LAXS experiments show that the structural transition from inherent TFE structure to the tetrahedral-like structure of water takes place between $x_{TFE} = 0.1$ and 0.2.

To quantitatively analyze the structure of pure TFE and the TFE−water mixtures, the experimental structure function and the theoretical one based on a plausible structure model were compared by using a least-squares refinement procedure. First, the structure parameter values of the intramolecular interactions within a TFE molecule were searched to explain the peaks in the *r*-space for pure TFE, such as 1.4 and 2.3 Å ones, on the basis of the values previously determined by the LAXS investigation.[29] Table 1 shows the obtained structure parameter values of the intramolecular interactions within a TFE molecule, but they were not refined by using a least-squares refinement

TABLE 2: Important Optimized Parameter Values of the Interactions in Water, TFE, and Their Mixtures Obtained by Least-Squares Fits[a]

		x_{TFE}													
interaction	parameter	0[b]	0.002	0.01	0.05	0.1	0.2	0.3	0.4	0.5	0.6	0.7	0.8	0.9	1
Linear Hydrogen Bond of Water−Water, TFE−Water, and TFE−TFE															
O···O	*r*	2.826(2)	2.855(3)	2.849(4)	2.841(3)	2.838(3)	2.830(3)	2.821(4)	2.816(5)	2.809(5)	2.805(6)	2.799(8)	2.799(9)	2.793(10)	2.799(8)
	10^3b	17	17	17	16	15	15	12	9	8	8	8	8	8	4
	n	3.43(3)	3.51(7)	3.30(6)	3.40(6)	3.32(5)	3.26(6)	2.82(5)	2.54(7)	2.33(6)	2.06(7)	1.86(9)	1.89(11)	1.95(12)	1.91(10)
Interstitial Water Molecules															
O···O	*r*	3.35	3.35	3.35	3.35	3.35	3.35	3.35	3.35	3.35					
	10^3b	15	15	15	15	15	15	15	15	15					
	n	1.0	1.0	1.0	1.0	1.0	1.0	1.0	1.0	1.0					
Second Neighbor of Water−Water, TFE−Water, and TFE−TFE															
O···O	*r*	4.50	4.55	4.55	4.55	4.55	4.55	4.55	4.55	4.55	4.55	4.55	4.55	4.55	4.60
	10^3b	90	90	90	90	90	90	90	90	90	90	90	90	90	30
	n	1.5	2.0	2.0	2.0	2.0	2.0	2.0	2.0	2.0	2.0	2.0	2.0	2.0	0.5
Water around the CF_3 Group of TFE															
F···O	*r*		3.225	3.225	3.225	3.225	3.225	3.225	3.225	3.225	3.225	3.225	3.225	3.225	
	10^3b		20	20	20	20	20	20	20	20	20	20	20	20	
	n		5.5	5.5	5.5	3.0	1.75	1.0	0.6	0.3	0.2	0.1	0.05	0.025	
C_2···O	*r*		3.775	3.775	3.775	3.775	3.775	3.775	3.775	3.775	3.775	3.775	3.775	3.775	
	10^3b		20	20	20	20	20	20	20	20	20	20	20	20	
	n		5.5	5.5	5.5	3.0	1.85	1.000	0.6	0.3	0.2	0.1	0.05	0.030	
First Neighbor of TFE-TFE															
O···F	*r*		3.02	3.02	3.02	3.02	3.02	3.02	3.02	3.02	3.02	3.02	3.02	3.02	3.02
	10^3b		20	20	20	20	20	20	20	20	20	20	20	20	20
	n		2.05	2.05	2.05	2.05	2.05	2.05	2.05	2.05	2.05	2.05	2.05	2.05	2.05
C_1···F	*r*		3.30	3.30	3.30	3.30	3.30	3.30	3.30	3.30	3.30	3.30	3.30	3.30	3.30
	10^3b		24	24	24	24	24	24	24	24	24	24	24	24	24
	n		0.7	0.7	0.7	0.7	0.7	0.7	0.7	0.7	0.7	0.7	0.7	0.7	0.7
C_1···F,C_2···F	*r*		4.95	4.95	4.95	4.95	4.95	4.95	4.95	4.95	4.95	4.95	4.95	4.95	4.95
	10^3b		30	30	30	30	30	30	30	30	30	30	30	30	30
	n		2.0	2.0	2.0	2.0	2.0	2.0	2.0	2.0	2.0	2.0	2.0	2.0	2.0
Second Neighbor of TFE-TFE															
O···F	*r*		3.80	3.80	3.80	3.80	3.80	3.80	3.80	3.80	3.80	3.80	3.80	3.80	3.80
	10^3b		25	25	25	25	25	25	25	25	25	25	25	25	25
	n		0.7	0.7	0.7	0.7	0.7	0.7	0.7	0.7	0.7	0.7	0.7	0.7	0.7
First and Second Neighbors of TFE−TFE															
F···F	*r*		5.50	5.50	5.50	5.50	5.50	5.50	5.50	5.50	5.50	5.50	5.50	5.50	5.50
	10^3b		40	40	40	40	40	40	40	40	40	40	40	40	40
	n		3.0	3.0	3.0	3.0	3.0	3.0	3.0	3.0	3.0	3.0	3.0	3.0	3.0

[a] The interatomic distance *r* (Å), the temperature factor *b* (Å^2), the number of interactions *n* per TFE molecule. The values in parentheses are standard deviations of the last figure. The parameters without standard deviations were not allowed to vary in the calculations. [b]Reference 28.

procedure in the present analysis. When the molar ratio for *g*-staggered and *g*-eclipsed conformations was assumed to be 1:1, the observed RDF for TFE could be explained well. Intermolecular interactions among TFE molecules in pure TFE were estimated by slightly modifying a trimer model proposed by Radnai et al.[29] In Figure 3, the modified trimer model is shown; three TFE molecules are hydrogen-bonded as the CF_3 groups are apart from each other due to its bulkiness. The structure parameter values of the modified trimer model reproduced well the experimental RDF for TFE at $r \leq \sim 7$ Å.

For the TFE−water mixtures, the structure parameter values of the intramolecular interactions for TFE and water molecules obtained from the above-mentioned analysis and the previous large-angle neutron scattering experiments,[32] respectively, were utilized. The structure parameter values of the modified trimer model and the tetrahedral-like structure of water, accompanied by nonbonding interstitial water molecules, were applied to search a plausible model. The experimental RDFs for the TFE−water mixtures could be explained by slightly modifying these structure parameter values. In the present analysis, the long-range interactions beyond ∼5.5 Å were not taken into account due to their complexity. Instead, a continuum electron distribution was assumed for the individual atoms. Finally, a least-squares fitting procedure was performed on the structure functions for TFE and the TFE−water mixtures over the *s* range from 0.1 to 14.4 $Å^{-1}$ to optimize the structure parameter values in the model. The structure parameter values of the intramolecular interactions for TFE and water molecules were not allowed to vary in the least-squares fitting. In Table 2, the important optimized values are summarized and shown in the structure model (Figure 3). All the structure parameter values for the intermolecular interactions for TFE and the TFE−water mixtures are listed in Table S2 in the Supporting Information. Figures 1 and 2 show that the theoretical *si*(*s*) and RDFs calculated by using the parameter values in Table S2 reproduce well the observed values, except for the long-range interactions at $s \leq \sim 3.5$ $Å^{-1}$ and $r > \sim 5.5-6.5$ Å not considered in the present analysis. The structure of pure TFE obtained agrees with that from the previous LAXS measurement by Radnai et al.[29]

For TFE the distance (2.799 ± 0.008 Å) of O···O hydrogen bonds is comparable with that (2.85 ± 0.01 Å) for ethanol estimated by a peak separation procedure in the *r*-space in the previous investigation.[17] The number (1.91 ± 0.10) of O···O hydrogen bonds for TFE is also close to that (1.9 ± 0.1) for ethanol.[17] These results reveal that TFE molecules form hydrogen-bonded chain clusters in the liquid as well as ethanol ones. As seen in Table 2, the distance of O···O hydrogen bonds for the TFE−water mixtures gradually increases with decreasing x_{TFE} (with increasing water content). The same tendency was observed for aqueous mixtures of aliphatic alcohols;[28,33,34] the O···O distance between water molecules in the tetrahedral-like structure of water, where one water molecule is bound with four water molecules, may be slightly longer than that between alcohol molecules in a chainlike structure of alcohol. Hence, the increase in the O···O distance suggests that the tetrahedral-like structure of water is gradually evolved in the TFE−water mixtures when the water content increases.

Figure 4 shows the number of O···O hydrogen bonds for the TFE−water mixtures as a function of alcohol mole fraction x_{alc}, together with that for ethanol−water mixtures estimated by a peak separation procedure in the *r*-space for comparison.[17] As seen in Figure 4, the number of O···O hydrogen bonds for the TFE−water mixtures does not significantly change with decreasing x_{TFE} from 1 to 0.7. On the other hand, that for ethanol−water mixtures markedly increases by addition of water to ethanol. This significant difference between the TFE−water and ethanol−water mixtures may be attributed to the very lower electrondonicity of the hydroxyl group of TFE molecule than that for ethanol one due to the electronegativity of F atoms. In fact, the donor number D_N for TFE is still ambiguous due probably to its very small value, while that for ethanol is 20.[35] The acceptor number A_N (53.3) for TFE[36] is larger than that (37.1) for ethanol.[35] The unbalance between donicity and acceptability of TFE molecule will be disadvantage to form hydrogen bonds with water molecules in the TFE−water mixtures. On the other hand, ethanol molecules can be hydrogen-bonded easily with water molecules as both hydrogen donor and hydrogen acceptor.[15−17] When the water content increases from $x_{TFE} = 0.6$ to 0.2, the number of O···O hydrogen bonds for the TFE−water mixtures significantly increases, suggesting that the tetrahedral-like structure of water is gradually evolved in the mixtures with increasing water content. In the range of $x_{TFE} < \sim 0.2$, the number of O···O hydrogen bonds is comparable with that for bulk water. Consequently, two break points at $x_{TFE} \approx 0.2$ and 0.7 appear in the plot of the number of O···O hydrogen bonds for the TFE−water mixtures against x_{TFE}. The former is comparable with that for ethanol−water mixtures.[17] It is suggested that the structural transition from the inherent TFE structure to the tetrahedral-like structure of water takes place in the TFE−water mixtures at $x_{TFE} \approx 0.2$ as well as in ethanol−water mixtures.

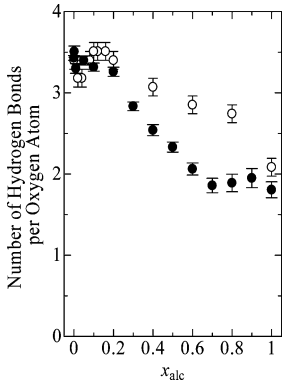

Figure 4. Coordination numbers per oxygen atom within alcohol and water molecules for TFE−water (filled circle) and ethanol−water[17] (opened circle) mixtures as a function of alcohol mole fraction x_{alc}. The standard deviations σ were indicated as error bars.

However, it should be noted that when $x_{TFE} > \sim 0.2$ the number of O···O hydrogen bonds for the TFE−water mixtures more rapidly decreases than that for ethanol−water mixtures. This suggests that the tetrahedral-like structure of water is more promptly disrupted in the TFE−water mixtures with increasing x_{TFE} due to the larger CF_3 group of TFE molecule than the ethyl group of ethanol one. The prompt disruption of the water structure in the TFE−water mixtures is demonstrated from the two other structure parameters listed in Table 2. The distance of O···O hydrogen bonds for the TFE−water mixtures in the range of $0.002 \leq x_{TFE} \leq 0.1$, where the tetrahedral-like structure of water is dominant, is elongated from that for pure water beyond the experimental uncertainties. This tendency was not found for aqueous mixtures of aliphatic alcohols previously investigated.[17,28,33,34] It is probable that O···O hydrogen bonds among water molecules are already weakened when TFE is added into water even at $x_{TFE} = 0.002$. Although the number of nonbonding interstitial water molecules for the TFE−water mixtures could not be optimized by the least-squares refinement procedure due to overlap of the TFE-TFE intermolecular

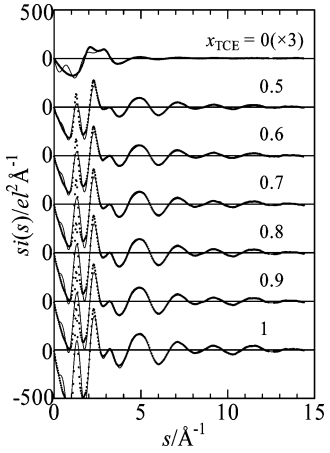

Figure 5. Structure functions $i(s)$ multiplied by s for TCE, water, and TCE−water mixtures at various x_{TCE}. Dotted lines represent experimental values, and solid lines are theoretical ones. The value in parentheses is a multiplication factor applied to the original one for clarity.

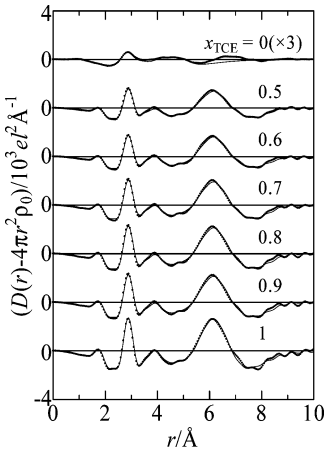

Figure 6. RDFs in the $D(r)$-$4\pi r^2\rho_0$ form for TCE, water, and TCE−water mixtures at various x_{TCE}. Dotted lines represent experimental values, and solid lines are theoretical ones.

interactions, such as $C_1\cdots F$, to the interaction of interstitial water molecules, the values show the presence of the interstitial water molecules in the TFE−water mixtures in the range of $0 \le x_{TFE} \le 0.5$. On the other hand, the interstitial water molecules were observed in ethanol−water mixtures in the wider range of $0 \le x_{EtOH} \le 0.6$ as described in the previous investigation.[17] This difference between the TFE−water and ethanol−water mixtures also shows that the water structure in the TFE−water mixtures is more rapidly disrupted with increasing x_{TFE} than those in ethanol−water mixtures.

The present results from the LAXS measurements show the structural change in the solvent clusters formed in the TFE−water mixtures with TFE mole fraction as follows: (1) TFE molecules form clusters via hydrogen bonding in pure TFE, and (2) the tetrahedral-like structure of water is gradually evolved in the mixtures at $x_{TFE} < \sim 0.7$, and both TFE clusters and water clusters coexist in the mixtures in the range of $\sim 0.2 < x_{TFE} < \sim 0.7$, (3) but the water clusters predominates in the mixtures at $x_{TFE} < \sim 0.2$.

LAXS for TCE—Water Mixtures. In Figure 5, the s-weighted structure functions $i(s)$ for pure TCE and the TCE−water mixtures in the TCE mole fraction range of $0.5 \le x_{TCE} \le 0.9$ are depicted, together with that for pure water[28] for comparison. Figure 6 shows the corresponding RDFs in the $D(r) - 4\pi r^2\rho_0$ form.

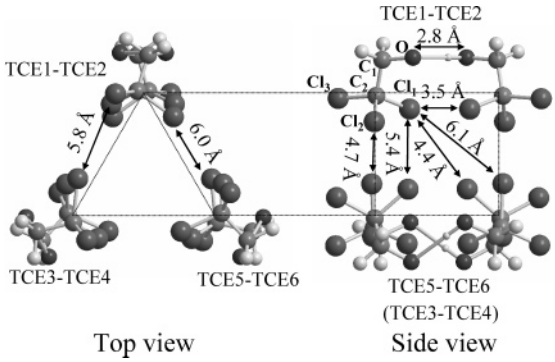

Figure 7. Structural model of the TCE cluster.

In the RDF for pure TCE ($x_{TCE} = 1$) a peak at 1.8 Å is mainly assigned to the C_2−Cl bond within a TCE molecule (Figure 7 shows the notation of atoms). A sharp peak at 2.9 Å arises from Cl···Cl and $C_1\cdots$Cl nonbonding interactions within a TCE molecule. Moreover, peaks at 2.9 and 3.9 Å can be assigned to $O\cdots Cl_{1,2}$ and $O\cdots Cl_3$ nonbonding interactions in a g-staggered conformation of TCE molecule, respectively. The intramolecular interactions of C_1-C_2 and C_1-O bonds and $C_2\cdots O$ nonbonding interaction should appear at 1.4 and 2.4 Å. However, the contribution of C−C and C−O interactions to the RDF for TCE is very small because interactions related to Cl atoms are large due to the very larger X-ray scattering factor of Cl atom than C and O ones. Therefore, O···O interactions between TCE molecules by hydrogen bonding are superimposed into the larger Cl···Cl and $C_1\cdots$Cl interactions at 2.9 Å. For the intermolecular interactions, the 3.9 Å peak is assigned to the first-neighbors between TCE molecules, such as Cl···C. A large peak centered at ∼6.1 Å corresponds to the second- and third-neighbor interactions of TCE molecules.

The RDFs for the TCE−water mixtures in the TCE mole fraction range of $0.5 \le x_{TCE} \le 0.9$ are comparable with that for pure TCE though the amplitudes of the intermolecular interactions at 3.9 and ∼6.1 Å decrease with decreasing x_{TCE}. This suggests that inherent TCE structure is kept in the TCE−water mixtures at $0.5 \le x_{TCE} \le 0.9$. This result and the fact that water is not miscible with TCE at $x_{TCE} < 0.5$ imply that water molecules may be embedded into vacancies of the TCE structure.

To clarify the structure of pure TCE at the molecular level, first, intramolecular interactions within a TCE molecule were built up by modifying those obtained from an ab initio investigation[37] to reproduce the peaks at 1.8, 2.8, and 3.9 Å in the r-space. The intramolecular parameter values are listed in Table 3, but were not refined by using a least-squares fitting procedure on the structure−function. This shows that TCE molecule has a g-staggered conformation in pure TCE, while TFE molecule has both g-staggered and g-eclipsed conformations at the 1:1 ratio in the liquid. It is probable that a g-eclipsed conformation for TCE molecule causes a large steric hindrance of Cl atoms for the hydroxyl O atom rather than that of F atoms. A plausible structure model for the intermolecular interactions was constructed in a trial-and-error manner in the r-space over the range of $r/Å \le 7$. The structure model obtained is depicted in Figure 7. As seen in the model, TCE molecules form a dimer through hydrogen bonding. Additionally, three dimers aggregate a triangle shape of cluster, where the CCl_3 groups are arranged on the corners of a triangle, interact among them due to van der Waals force. For the TCE−water mixtures a combination of the inherent TCE structure and the tetrahedral-like structure

TABLE 3: Intramolecular Interactions for TCE Molecule[a]

interaction	*r*	10^3b	*n*
2,2,2-Trichloroethanol			
O−H	0.960	2	1.0
C_1−H	1.085	1	2.0
C_2−Cl	1.760	2	3.0
C_1−O	1.410	3	1.0
C_1−C_2	1.510	2	1.0
H···H	1.770	5	1.0
C_2···H	2.130	9	2.0
Cl···Cl	2.875	4.8	3.0
C_1···Cl	2.673	6	3.0
C_2···O	2.385	6	1.0
g-Staggered Conformer			
O···Cl_1,Cl_2	2.985	35	2.0
O···Cl_3	3.941	20	1.0
H···H	1.518	10	1.0

[a] The distance *r* (Å), temperature factor *b* (Å^2), and number *n*.

TABLE 4: Important Parameter Values of the Interactions in TCE and TCE−Water Mixtures at $0.5 \leq x_{TCE} \leq 0.9$ Obtained by Least-Squares Fits[a]

		x_{TCE}					
iinteraction	parameter	0.5	0.6	0.7	0.8	0.9	1
Linear Hydrogen Bond of Water−Water, TCE−Water, and TCE−TCE							
O···O	*r*	2.890	2.897	2.897	2.897	2.897	2.897
	10^3b	8	10	10	9	8	8
	n	3.16	3.10	2.80	1.95	0.90	0.8
Second Neighbor of Water−Water and TCE−TCE							
O···O	*r*	4.55	4.55	4.55	4.55	4.55	
	10^3b	90	90	90	90	90	
	n	1.5	1.5	1.5	1.5	1.5	
Water around the CCl_3 Group of TCE							
Cl···O	*r*	3.80	3.80	3.80			
	10^3b	30	30	30			
	n	0.4	0.75	0.50			
Interactions of Hydrogen-Bonded TCE−TCE							
O···Cl_3	*r*	3.07	3.07	3.07	3.07	3.07	3.07
	10^3b	30	30	30	30	30	30
	n	0.8	0.8	0.8	0.8	0.8	0.8
Cl_3···Cl_3	*r*	3.463	3.463	3.463	3.463	3.463	3.463
	10^3b	10	10	10	10	10	10
	n	0.4	0.4	0.4	0.4	0.4	0.4
Cl_2···Cl_3	*r*	3.817	3.817	3.817	3.817	3.817	3.817
	10^3b	10	10	10	10	10	10
	n	0.8	0.8	0.8	0.8	0.8	0.8
Interactions Between Hydrogen-Bonded TCE Dimers							
Cl_2···Cl_2	*r*	4.71	4.71	4.71	4.71	4.71	4.71
	10^3b	45	45	45	45	45	45
	n	0.4	0.4	0.4	0.4	0.4	0.4
Cl_3···Cl_3	*r*	5.354	5.354	5.354	5.354	5.354	5.354
	10^3b	40	40	40	40	40	40
	n	0.4	0.4	0.4	0.4	0.4	0.4
Interactions between Hydrogen-Bonded TCE Dimers							
Cl_3···Cl_3	*r*	4.377	4.377	4.377	4.377	4.377	4.377
	10^3b	10	10	10	10	10	10
	n	0.32	0.32	0.32	0.32	0.32	0.32
Cl_1···Cl_3,	*r*	6.159	6.159	6.159	6.159	6.159	6.159
Cl_2···Cl_3	10^3b	60	60	60	60	60	60
	n	0.72	0.72	0.72	0.72	0.72	0.72

[a] The interatomic distance *r* (Å), the temperature factor *b* (Å^2), the number of interactions *n* per TCE molecule, and the continuum electron distribution *R* (Å) and *B* (Å^2). The values in parentheses are standard deviations of the last figure. The parameters without standard deviations were not allowed to vary in the calculations.

of water with nonbonding interstitial water molecules was used as a structure model. Indeed, the model could explain well the experimental values in the *r*-space.

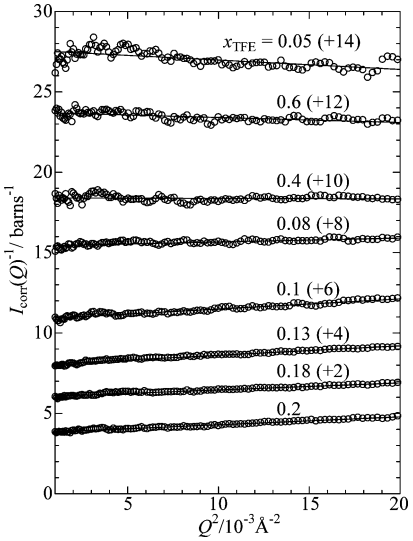

Figure 8. Ornstein−Zernike plots of the SANS intensities for the TFE-d_1−D_2O mixtures at various x_{TFE}. Circles represent the experimental values and solid lines the theoretical ones. The values in parentheses are those shifted from the origin to avoid overlap of the plots.

A least-squares fitting procedure was performed on the structure functions for pure TCE and the TCE−water mixtures over the *s* range from 0.1 to 14.4 Å^{-1} by using the structure parameter values of the model. However, the structure parameter values for the O···O hydrogen bonds could not be optimized because of their small contribution to the RDFs for TCE and the TCE−water mixtures. In the present analysis, thus, the structure parameter values for a continuum electron distribution were only refined by using a least-squares refinement on the structure functions. The important structure parameter values are summarized in Table 4 and indicated in the structure model (Figure 7). In Table S4 in the Supporting Information, all the structure parameter values for the intermolecular interactions in TCE and the TCE−water mixtures were given. The theoretical *si*(*s*) and RDFs calculated by using the parameter values in Table 4S reproduce well the observed values in the range of $s > \sim 3.5$ Å^{-1} and $r < \sim 6.5$ Å, where the structure parameter values were built up. Although the structural parameters for O···O hydrogen bonds could not be optimized, Table 4 reveals the increase in the number of O···O hydrogen bonds for the TCE−water mixtures with increasing water content. This may be caused mainly by enhancement of O···O hydrogen bonds among water molecules in the mixtures with increasing water content, but TCE molecules may not be hydrogen-bonded with water ones due to the large hydrophobicity of the CCl_3 group. Actually, water is not miscible at 298 K with TCE in the range of $x_{TCE} < 0.5$.

SANS for TFE—Water Mixtures. Figures 8 and 9 show Ornstein−Zernike plots of the normalized SANS intensities for the TFE-d_1−D_2O and TFE-d_2−H_2O mixtures at various TFE mole fractions, respectively; the reciprocal intensities for the mixtures are plotted as a function of Q^2 in the range of $1 \times 10^{-3} \leq Q^2/\text{Å}^{-1} \leq 2 \times 10^{-2}$. The SANS intensities of the TFE-d_1−D_2O mixtures mainly give us information on clustering of water molecules due to the larger neutron scattering length (6.671 fm) of the D atom than that (−3.739 fm) of the H one, whereas those for the TFE-d_2−H_2O mixtures mainly show clustering of TFE molecules.

As shown in Figure 8, the slopes of the reciprocal SANS intensities for the TFE-d_1−D_2O mixtures against Q^2 are obviously positive in the range of $0.1 \leq x_{TFE} \leq 0.2$, but almost flat or slightly negative in the ranges of $x_{TFE} \leq 0.08$ and $x_{TFE} \geq$

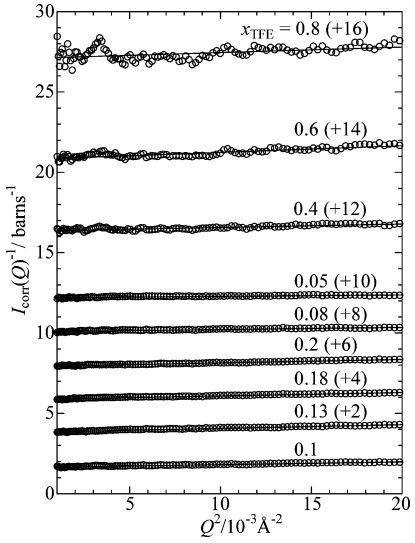

Figure 9. Ornstein−Zernike plots of the SANS intensities for the TFE-d_2−H_2O mixtures at various x_{TFE}. Circles represent the experimental values and solid lines the theoretical ones. The values in parentheses are those shifted from the origin to avoid overlap of the plots.

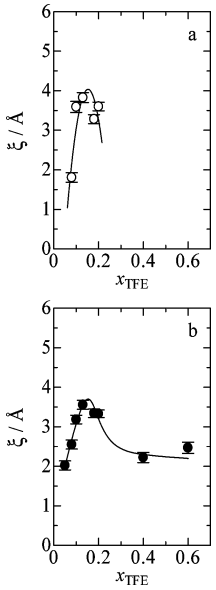

Figure 10. Correlation lengths ξ for (a) TFE-d_1−D_2O and (b) TFE-d_2−H_2O mixtures as a function of TFE mole fraction. The solid lines are drawn to clarify their variation. The standard deviations σ were indicated as error bars.

0.4. In addition, the experimental values for the TFE-d_1−D_2O mixtures at $x_{TFE} = 0.05$, 0.4, and 0.6 are slightly dispersed, showing that the SANS intensities are weak at the mole fractions. These features show that the concentration fluctuation in the TFE-d_1−D_2O mixtures is enhanced in the narrow range of $0.1 \leq x_{TFE} \leq 0.2$, i.e., D_2O clusters are evolved in the mixtures in this range. Figure 9 reveals less significant difference among the slopes of the reciprocal SANS intensities for the TFE-d_2−H_2O mixtures at the mole fractions investigated. However, the dispersed experimental values for the mixtures at $x_{TFE} = 0.6$ and 0.8 indicate their weak SANS intensities. On the other hand, the experimental values for the TFE-d_2−H_2O mixtures in the range of $0.05 \leq x_{TFE} \leq 0.2$ are not dispersed, and their slopes are positive. It is suggested that formation of TFE clusters progresses in the mixtures in this range. These results for the TFE-d_1−D_2O and TFE-d_2−H_2O mixtures are consistent with each other; both TFE clusters and water clusters are most enhanced in TFE−water mixtures in the narrow range of $0.1 \leq x_{TFE} \leq 0.2$, i.e., TFE and water molecules are inhomogeneously mixed in this range.

To make a quantitative analysis on the SANS intensities for the TFE-d_1−D_2O and TFE-d_2−H_2O mixtures, the reciprocal intensities as a function of Q^2 are fitted by a least-squares refinement procedure using the Ornstein−Zernike[38] equation,

$$I_{corr}(Q)^{-1} = I(0)^{-1}[1 + \xi^2 Q^2] \quad (1)$$

where ξ represents the Ornstein−Zernike correlation length. As seen in Figures 8 and 9, the theoretical values (solid line) obtained from the least-squares fits reproduce the experimental ones. In Table 5, the optimized correlation lengths are listed. For the TFE-d_1−D_2O mixtures at $x_{TFE} = 0.05$, 0.4, and 0.6 and the TFE-d_2−H_2O mixture at $x_{TFE} = 0.8$ the correlation lengths could not be obtained with reasonable reliability because of their weak SANS intensities. Parts a and b of Figure 10 show the correlation lengths ξ for the TFE-d_1−D_2O and TFE-d_2−H_2O mixtures as a function of x_{TFE}, respectively. The correlation lengths ξ for the TFE-d_1−D_2O mixtures as a function of x_{TFE} have a sharp peak at $x_{TFE} \approx 0.15$ with $\xi \approx 4$ Å. A similar tendency is observed in the correlation length for the TFE-d_2−H_2O mixtures as a function of x_{TFE}. These findings clearly show

TABLE 5: Correlation Lengths ξ (Å) for TFE-d_1−D_2O and TFE-d_2−H_2O Mixtures as a Function of TFE Mole Fraction Obtained from the SANS Measurements

x_{TFE}	ξ(TFE-d_1-D_2O)	ξ(TFE-d_2−H_2O)
0.05		2.02(11)
0.08	1.81(12)	2.55(11)
0.1	3.59(14)	3.18(11)
0.13	3.83(12)	3.56(12)
0.18	3.28(11)	3.34(11)
0.2	3.60(11)	3.33(10)
0.4		2.22(13)
0.6		2.47(14)

that TFE clusters and water clusters are most significantly evolved in the mixtures at $x_{TFE} \approx 0.15$. The maximum at $x_{TFE} \approx 0.15$ is close to the break point at $x_{TFE} = 0.2$ in the number of O···O hydrogen bonds determined from the LAXS experiments, where the structural transition from the inherent TFE structure to the tetrahedral-like structure of water takes place.

The previous SAXS[39] and SANS[40] investigations on ethanol−water mixtures revealed weaker scattering intensities than those for the TFE−water mixtures, suggesting that the concentration fluctuation for ethanol−water mixtures is less significant than for TFE−water ones. Thus, the larger hydrophobicity for the CF_3 group of TFE molecule induces the heterogeneities of the TFE−water mixtures. On the other hand, the previous investigation on HFIP−water mixtures showed that the correlation length ξ reaches a maximum at $x_{HFIP} = 0.071$ with $\xi \approx 10$ Å.[12] Hence, HFIP molecules lead to more rapid and significant clustering of HFIP molecules than TFE molecules when HFIP is added into water. This is caused by the larger size and the more CF_3 groups of HFIP molecule than TFE one. Thus, the 2-propanol skeleton is larger than the ethanol one. In fact, the SAXS investigations indicated that the concentration fluctuation for 2-propanol−water mixtures[41] is larger by a factor of ~6 than that for ethanol−water mixtures.[39] In addition, two hydrophobic CF_3 groups of HFIP molecule may lead enhancement of clustering of HFIP molecules in HFIP−water mixtures.

^{1}H NMR Relaxation. The ^{1}H NMR relaxation rates R_1 ($= T_1^{-1}$) for the methylene (CH_2) group of TFE and ethanol molecules in the TFE−water and ethanol−water mixtures are

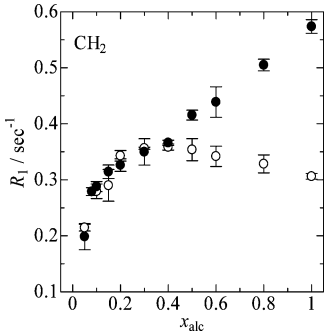

Figure 11. ^{1}H NMR relaxation rates R_1 for the methylene (CH_2) group of TFE and ethanol molecules in TFE−water (filled circles) and ethanol−water (open circles) mixtures. The standard deviations σ were indicated as error bars.

TABLE 6: ^{1}H NMR Relaxation Rates R_1 for Methylene Groups of TFE and Ethanol Molecules in TFE−Water and Ethanol−Water Mixtures at Various Mole Fractions

TFE-water		ethanol−water	
x_{TFE}	R_1/s^{-1}	x_{EtOH}	R_1/s^{-1}
0.05	0.199(23)	0.05	0.215(6)
0.08	0.279(23)		
0.1	0.288(9)	0.1	0.280(13)
0.15	0.314(12)	0.15	0.290(28)
0.2	0.326(11)	0.2	0.343(9)
0.3	0.350(24)	0.3	0.356(2)
0.4	0.366(5)	0.4	0.358(6)
0.5	0.415(9)	0.5	0.354(20)
0.6	0.439(27)	0.6	0.342(18)
0.8	0.505(10)	0.8	0.328(16)
1	0.574(12)	1	0.306(5)

given in Table 6 and plotted as a function of alcohol mole fraction x_{alc} in Figure 11. In the neat alcohols, the ^{1}H relaxation for the CH_2 group of alcohol molecules is governed mainly with intramolecular and intermolecular ^{1}H−^{1}H dipole interactions. In the alcohol−water mixtures, on the other hand, the intermolecular ^{1}H−^{1}H dipole interaction between alcohol and water molecules also contributes to the ^{1}H relaxation for the CH_2 group. Furthermore, the intramolecular and intermolecular ^{1}H−^{19}F dipole interactions may affect the relaxation in the TFE−water mixtures. Therefore, the relaxation rates measured for the CH_2 group in both mixtures involve complex information on the translational and rotational motions of alcohol molecules in the mixtures.[42,43] Nevertheless, Figure 11 shows interesting features of the R_1 values for the CH_2 groups of TFE and ethanol molecules in both mixtures. For the TFE−water mixtures the R_1 values for the CH_2 group monotonically decrease with decreasing x_{TFE} from 1 to 0.15 and then do more quickly when the mole fraction is further decreased; i.e., a break point appears at $x_{TFE} \approx 0.15$. This agrees with those in the number of hydrogen bonds and the Ornstein−Zernike correlation length ξ determined by the present LAXS and SANS experiments, respectively. On the other hand, for the ethanol−water mixtures the R_1 value for the CH_2 group slightly increases when the x_{EtOH} decreases from 1 to ∼0.3 and decreases with further decreasing x_{EtOH}. It results in a maximum at $x_{EtOH} \approx 0.3$, which is close to a break point at $x_{EtOH} = 0.2$ in the number of hydrogen bonds and the average hydration number of ethanol clusters as a function of x_{EtOH} obtained from the previous LAXS and mass spectrometric experiments, respectively.[15−17] It is thus shown that both points at $x_{TFE} \approx 0.15$ and $x_{EtOH} \approx 0.3$ for the TFE−water and ethanol−water mixtures, respectively, reflect the structural transition from alcohol clusters to the tetrahedral-like structure of water at each mole fraction.

The difference between the changes in the R_1 values for the TFE−water and ethanol−water mixtures can be explained as follows. The R_1 value for pure TFE is twice as large as that for pure ethanol, suggesting that the motions of TFE molecule are slower than those of ethanol one. This is caused by the heavier TFE molecule as compared with the ethanol one; i.e., the molecular weight (100.04) for TFE is larger by a factor of ∼2 than that (46.07) of ethanol. In the ethanol−water mixtures at $0.2 < x_{EtOH} < 1$, as concluded in the previous investigation,[15−17] ethanol clusters are predominantly formed and can easily interact with water molecules by hydrogen bonding. Hence, the motions of ethanol molecules in ethanol clusters may be gradually restricted with increasing water content, leading to the increase in the R_1 value from $x_{EtOH} = 1$ to ∼0.3. On the other hand, in the TFE−water mixtures at $\sim 0.15 < x_{TFE} < 1$, as discussed in the LAXS section, TFE molecules are less easily hydrogen-bonded with themselves and water molecules than ethanol ones because of the weak electrondonicity of the hydroxyl group of TFE molecule. Thus, the motions of TFE molecules in TFE clusters are not significantly retarded in the TFE−water mixtures with increasing water content, but gradually become free. Consequently, the R_1 value monotonically decreases with increasing water content from $x_{TFE} = 1$ to ∼0.15.

In the TFE−water and ethanol−water mixtures at $x_{TFE} < \sim 0.15$ and $x_{EtOH} < \sim 0.3$, respectively, where the tetrahedral-like structure of water predominates, the motions of both TFE and ethanol molecules rapidly become free with increasing water content due probably to an increase of alcohol monomers in the mixtures. Hence, the R_1 values for both mixtures drastically decrease with increasing water content.

Structure of TFE—Water and TCE—Water Mixtures. On the basis of all the results presented, a plausible structural change in solvent clusters predominantly formed in the TFE−water mixtures with TFE mole fraction is proposed as follows. In the range of $0.7 < x_{TFE} < 1$, the inherent TFE structure is dominant in the TFE−water mixtures. In the TFE structure, TFE molecules are hydrogen-bonded to other molecules as the CF_3 groups are apart from each other due to the steric hindrance. When the water content increases from $x_{TFE} \approx 0.7$, the tetrahedral-like structure of water is gradually evolved in the mixtures. TFE and water molecules are heterogeneously mixed with each other at the molecular level; both TFE and water clusters coexist in the TFE−water mixtures. This microheterogeneity is most enhanced in the TFE−water mixtures at $x_{TFE} \approx 0.15$. On the contrary, in the range of $x_{TFE} < \sim 0.15$ the tetrahedral-like structure of water predominates in the TFE−water mixtures, and TFE monomers may be hydrated in the water clusters. It is thus concluded that the structural transition from the inherent TFE structure to the tetrahedral-like structure of water takes place at $x_{TFE} \approx 0.15$. The structural transition point for the TFE−water mixture is slightly lower than that ($x_{EtOH} \approx 0.2$) for ethanol−water mixtures.[15−17] This arises from the larger CF_3 group of TFE molecule than the CH_3 group of ethanol one, i.e., the tetrahedral-like structure of water is quickly disrupted by addition of TFE to water.

Beyond the structural transition point ($x_{TFE} \geq \sim 0.15$), TFE molecules form their clusters in the TFE−water mixtures. Here, a driving force of the clustering may be the hydrophobic interaction among the CF_3 groups rather than hydrogen bonding between TFE molecules because of the weak hydrogen-bond acceptor (low electrondonicity) of the hydroxyl group due to the strong electrondrawing of F atoms. From the same reason TFE molecules cannot be strongly hydrogen-bonded with water molecules. On the other hand, the ethanol molecule can be easily

hydrogen-bonded with other ethanol molecules and water ones due to the suitable abilities for hydrogen-bond acceptor and donor of the hydroxyl group. Thus, the microheterogeneity of the TFE−water mixtures is more significant than that for ethanol−water mixtures. The weaker intermolecular interactions between TFE molecules than ethanol ones influence the dynamics of TFE molecules in the TFE−water mixtures. The motions of TFE molecules in TFE clusters gradually become free with increasing water content, while those of ethanol molecules in ethanol clusters are retarded with increasing water content probably because ethanol clusters are strengthened by hydration of water molecules. For HFIP−water mixtures, the further large hydrophobic group of HFIP molecule than TFE one together with the weak hydrogen-bond acceptor of the hydroxyl group lead to the lower structural transition point ($x_{HFIP} \approx 0.1$) and the more significant microheterogeneity than that for the TFE−water mixtures.[12]

In the TCE−water mixtures, the inherent TCE structure remains in the range of $0.5 \leq x_{TCE} < 1$. In the TCE structure, TCE molecules form dimers by hydrogen bonding, but not chainlike clusters. Additionally, the dimers aggregate with the hydrophobic interactions among the CCl_3 groups. This is attributed to that hydrogen bonds between TCE molecules cannot be easily formed due to the steric hindrance of the very large CCl_3 group and the weak hydrogen-bond acceptor of the hydroxyl group. The two factors lead to that water molecules are not miscible with TCE molecules at $x_{TCE} < 0.5$. In the range of $0.5 \leq x_{TCE} < 1$, water molecules will exist in vacancies of the TCE structure.

Acknowledgment. This work was supported partly by Grants-in-Aid (No. 15550016 to T.T. and No. 15076211 to T.Y.) from the Ministry of Education, Culture, Sports, Science, and Technology, Japan.

Supporting Information Available: All the optimized structure parameters obtained from the present LAXS experiments (Tables S2 and S4). This material is available free of charge via the Internet at http://pubs.acs.org.

References and Notes

(1) Sonnichsen, S. P.; van Eyk, J. E.; Hodges, R. S.; Sykes, B. D. *Biochemistry* **1992**, *31*, 8790.
(2) Narhi, L. O.; Philo, J. S.; Li, T. S.; Zhang, M.; Samal, B.; Arakawa, T. *Biochemistry* **1996**, *35*, 11447.
(3) Buck, M.; Schwalbe, H.; Dobson, C. M. *J. Mol. Biol.* **1996**, *257*, 669.
(4) Lu, H.; Buck, M.; Radford, S. E.; Dobson, C. M. *J. Mol. Biol.* **1997,** *265*, 112.
(5) Buck, M. *Rev. Biophys.* **1998**, *31*, 297.
(6) Luo, Y. Z.; Baldwin, R. L. *J. Mol. Biol.* **1998**, *279*, 49.
(7) Reierson, H.; Rees, A. R. *Protein Eng.* **2000**, *13*, 739.
(8) Wood, S. J.; Maleeff, B.; Hart, T.; Wetzel, R. *J. Mol. Biol.* **1996**, *256*, 870.
(9) Hirota, N.; Mizuno, K.; Goto, Y. *Protein Sci.* **1997**, *6*, 416.
(10) Hirota, N.; Mizuno, K.; Goto, *J. Mol. Biol.* **1998**, *275*, 365.
(11) Hong, D.-P.; Hoshino, M.; Kuboi, R.; Goto, Y. *J. Am. Chem. Soc.* **1999**, *121*, 8427.
(12) Yoshida, K.; Yamaguchi, T.; Adachi, T.; Otomo, T.; Matsuo, D.; Takamuku, T.; Nishi, N. *J. Chem. Phys.* **2003**, *119*, 6132.
(13) Johansson, J. S.; Solt, K.; Reddy, K. S. *Photochem. Photobiol.* **2003**, *77*, 89.
(14) Jackson, M.; Mantsch, H. H. *Biochim. Biophys. Acta* **1992**, *1118*, 139.
(15) Nishi, N.; Takahashi, S.; Matsumoto, M.; Tanaka, A.; Muraya, K.; Takamuku, T.; Yamaguchi, T. *J. Phys. Chem.* **1995**, *99*, 462.
(16) Matsumoto, M.; Nishi, N.; Furusawa, T.; Saita, M.; Takamuku, T.; Yamagami, M.; Yamaguchi, T. *Bull. Chem. Soc. Jpn.* **1995**, *68*, 1775.
(17) (a) Nishi, N.; Matsumoto, M.; Takahashi, S.; Takamuku, T.; Yamagami, M.; Yamaguchi, T. *Structures and Dynamics of Clusters*; Kondow, T., Kaya, K., Terasaki, A., Eds.; Universal Academy Press, Inc. and Yamada Science Foundation: 1996; pp 113−120. (b) Matsumoto, M. Master's Thesis, Kyushu University, 1996.
(18) Yamanaka, K.; Yamaguchi, T.; Wakita, H. *J. Chem. Phys.* **1994**, *101*, 9830.
(19) Ihara, M.; Yamaguchi, T.; Wakita, H.; Matsumoto, T. *Adv. X-ray Anal. Jpn.* **1994**, *25*, 49. Yamaguchi, T.; Wakita, H.; Yamanaka, K. *Fukuoka Univ. Sci. Rep.***1999**, *29*, 127.
(20) Furukawa, K. *Rep. Progr. Phys.* **1962**, *25*, 395.
(21) Krogh-Moe, J. *Acta Crystallogr.* **1956**, *2*, 951.
(22) Norman, N. *Acta Crystallogr.* **1957**, *10*, 370.
(23) Takamuku, T.; Tabata, M.; Yamaguchi, A.; Nishimoto, J.; Kumamoto, M.; Wakita, H.; Yamaguchi, T. *J. Phys. Chem. B* **1998**, *102*, 8880.
(24) Johanson, G.; Sandström, M. *Chem. Scr.* **1973**, *4*, 195.
(25) Yamaguchi, T. Doctoral Thesis, Tokyo Institute of Technology, 1978.
(26) Otomo, T.; Furusaka, M.; Satoh, S.; Itoh, S.; Adachi, T.; Shimizu, S.; Takeda, M. *J. Phys. Chem. Solids* **1999**, *60*, 1579.
(27) Sears, V. F. *Thermal-Neutron Scattering Lengths and Cross Sections for Condensed-Matter Research*; Chalk River Lab.: Chalk River, Ontario, Canada, 1984.
(28) Takamuku, T.; Yamaguchi, T.; Asato, M.; Matsumoto, M.; Nishi, N. *Z. Naturforsch.* **2000**, *55a*, 513.
(29) Radnai, T.; Ishiguro, S.; Ohtaki, H. *J. Solution Chem.* **1989**, *18*, 8.
(30) Narten, A. H.; Levy, H. A. *J. Chem. Phys.* **1971**, *55*, 2263.
(31) Narten, A. H. *J. Chem. Phys.* **1972**, *56*, 5681.
(32) Ichikawa, K.; Kameda, Y.; Yamaguchi, T.; Wakita, H.; Misawa, M. *Mol. Phys.* **1991**, *73*, 79.
(33) Takamuku, T.; Maruyama, H.; Watanabe, K.; Yamaguchi, T. *J. Solution Chem.* **2004**, *33*, 537.
(34) Takamuku, T.; Saisho, K.; Aoki, S.; Yamaguchi, T. *Z. Naturforsch.* **2002**, *57a*, 982.
(35) Gutmann, V. *The Donor−Acceptor Approach to Molecular Interactions;* Plenum Press: New York, 1978.
(36) Mayer, U. *Stud. Phys. Theor. Chem.* **1983**, *27*, 219.
(37) Moulin, V.; Schriver, A.; Schriver-Mazzuoli, L.; Chaquin, P. *Chem. Phys. Lett.* **1996**, *263*, 423.
(38) Stanley, H. E. *Introduction to Phase Transitions and Critical Phenomena*; Clarendon Press: Oxford, England, 1971.
(39) Nishikawa, K.; Iijima, T. *J. Phys. Chem.* **1993**, *97*, 10824.
(40) D′Arrigo, G.; Teixeira, J. *J. Chem. Soc., Faraday Trans.* **1990**, *86*, 1503.
(41) Hayashi, H.; Nishikawa, K.; Iijima, T. *J. Phys. Chem.* **1990**, *94*, 8334.
(42) Bachl, F.; Lüdemann, H.-D. *High-Pressure Res.* **1990**, *6*, 91.
(43) Takamuku, T.; Hirano, T.; Yamaguchi, T.; Wakita, H. *J. Phys. Chem.* **1992**, *96*, 9487.